

Evolutionary BP+OSD Decoding for Low-Latency Quantum Error Correction

Hee-Youl Kwak¹, Seong-Joon Park², Hyunwoo Jung³, Jeongseok Ha³, and Jae-Won Kim⁴

¹Department of Electrical, Electronic and Computer Engineering, University of Ulsan, Ulsan, South Korea

²Institute of Artificial Intelligence, Pohang University of Science and Technology (POSTECH), Pohang, South Korea

³School of Electrical Engineering, Korea Advanced Institute of Science and Technology (KAIST), Daejeon, South Korea

⁴Department of Electronic Engineering, Gyeongsang National University, Jinju, South Korea

(Dated: December 23, 2025)

We propose an evolutionary belief propagation (EBP) decoder for quantum error correction, which incorporates trainable weights into the BP algorithm and optimizes them via the differential evolution algorithm. This approach enables end-to-end optimization of the EBP combined with ordered statistics decoding (OSD). Experimental results on surface codes and quantum low-density parity-check codes show that EBP+OSD achieves better decoding performance and lower computational complexity than BP+OSD, particularly under strict low latency constraints (within 5 BP iterations).

Introduction— Quantum computers promise computational capabilities beyond the reach of classical computers [1–4], but they face a fundamental challenge due to the high error rates of noisy quantum hardware. Quantum error correction (QEC) addresses this limitation by encoding logical information into many noisy physical qubits [5–7]. Recent advances in QEC have marked significant progress toward practical quantum computation [8–12].

A key requirement for practical QEC is achieving strong decoding performance within the coherence time of the quantum system, which demands extremely low latency and computational complexity [11–13]. From a complexity standpoint, the belief propagation (BP) decoder [14] is preferred for sparse codes such as the surface code [15–18] and quantum low-density parity-check (QLDPC) codes [9, 19–21], due to its linear complexity. However, its performance is limited by the quantum degeneracy inherent in quantum codes [22–24]. To address this limitation, hybrid schemes combining BP with ordered statistics decoding (OSD) have been proposed, where OSD provides a strong post-processing stage at the cost of high complexity [21, 25].

Machine learning-based decoders, including feed-forward networks (FFNs) [26], convolutional neural networks (CNNs) [27, 28], and transformers [29], have also been investigated. However, their high complexity limits scalability to large code lengths. In contrast, the neural BP (NBP) decoder introduces trainable weights into the BP algorithm while preserving linear complexity [30–32]. Despite this advantage, its performance still lags behind that of the BP+OSD decoder. Although NBP can be combined with OSD, end-to-end optimization is not feasible because OSD is non-differentiable.

In this letter, we propose an evolutionary BP (EBP) decoder. Similar to the NBP decoder, the EBP decoder employs trainable weights; however, the weights are optimized using the differential evolution (DE) algorithm [33, 34]. Unlike neural networks, DE can optimize non-differentiable objectives, enabling end-to-end optimization of the EBP+OSD structure with flexible objective functions. The optimization is designed to im-

prove decoding performance while reducing the activation probability of the computationally intensive OSD stage. Furthermore, we propose a weight sharing technique to improve optimization efficiency and allow weight reuse across the same code class.

Experimental results demonstrate that the proposed EBP+OSD decoder outperforms the conventional BP+OSD decoder for both surface codes and QLDPC codes in terms of logical error rate (LER) and threshold performance, while achieving lower decoding complexity through substantially fewer OSD activations. Notably, these gains are achieved under strict low-latency constraints, using only 5 BP iterations—far fewer than those used in prior studies (BP+OSD [21]: 32 iterations; BP with topological blocking decoder [35]: 20 iterations; BP with memory [36]: 150 iterations). Overall, the proposed decoder achieves a favorable balance between performance and complexity under limited-latency conditions, which is highly desirable for real-time decoding.

Quantum Codes—In this letter, we focus on stabilizer codes. An $[[n, k, d]]$ stabilizer code is defined by a stabilizer group $\mathcal{S} \subseteq \mathcal{P}^{\otimes n}$, where $\mathcal{P}^{\otimes n}$ denotes the n -qubit Pauli group. The codespace is the joint $+1$ eigenspace of all stabilizers, given by $\mathcal{C} = \{|\psi\rangle : S|\psi\rangle = |\psi\rangle, \forall S \in \mathcal{S}\}$. Here, k logical qubits are encoded into n physical qubits. Nontrivial logical operators are Pauli operators that commute with all stabilizers but are not elements of \mathcal{S} . They map one logical state to another, thereby corrupting the encoded information. The minimum distance d is the minimum weight among all non-trivial logical operators. In this work, we consider two representative code classes: the rotated surface code [18] with parameters $[[d^2, 1, d]]$, and the bivariate bicycle QLDPC codes [9] with parameters $[[72, 12, 6]]$, $[[90, 8, 10]]$, and $[[144, 12, 12]]$.

The stabilizer group \mathcal{S} can be represented by an $m \times n$ stabilizer matrix \mathbf{S} , where $m \geq n - k$. Each entry of \mathbf{S} corresponds to a Pauli element acting on a physical qubit. The i -th row of \mathbf{S} specifies the set of Pauli elements defining the stabilizer S_i . Given an error operator $\mathcal{E} \in \mathcal{P}^{\otimes n}$, the syndrome vector $\mathbf{s} = (s_1, \dots, s_m) \in \mathbb{F}_2^m$ is calculated by $s_i = \langle \mathcal{E}, S_i \rangle \in \mathbb{F}_2$, where $\langle \cdot, \cdot \rangle$ denotes the symplectic inner product, which equals 0 if the two operators com-

mute and 1 if they anticommute. This syndrome vector can be obtained by measuring ancilla qubits and then passed to the decoder for error correction.

Quantum BP Decoding— The decoding task is to estimate the most probable error operator $\hat{\mathcal{E}}$ from the observed syndrome \mathbf{s} . BP decoding is an iterative message-passing algorithm operating on a Tanner graph, which consists of n variable nodes (VNs) representing n physical qubits and m check nodes (CNs) representing m stabilizers. In quantum codes, BP can be implemented either as binary BP₂ [23] or as quaternary BP₄ [24]. NBP extends BP by introducing trainable weights [30], resulting in two variants: NBP₂ [31] and NBP₄ [32]. In this work, we focus on BP₄ and NBP₄, which we simply refer to as BP and NBP.

The NBP decoder operates as follows. Each VN v can take one of four states $\{I, X, Z, Y\}$. Under a depolarizing noise model with error probability p , the channel log-likelihood ratio (LLR) for VN v with error type $\zeta \in \{X, Z, Y\}$ is initialized as $L_{v(\zeta)} = \ln((1-p)/(p/3))$. Since the exact channel parameter p is often unknown and has limited impact on decoding performance [32], it is fixed to $p = 0.1$ for initialization. The decoder then performs iterative message passing for up to $\bar{\ell}$ iterations. At iteration ℓ , the message from VN v with error type ζ to CN c is computed by

$$m_{v(\zeta) \rightarrow c}^{(\ell)} = \bar{w}_v^{(\ell)} L_{v(\zeta)} + \sum_{\substack{c' \in \mathcal{N}(v) \setminus c \\ \langle \zeta, S_{c',v} \rangle = 1}} w_{c' \rightarrow v}^{(\ell)} m_{c' \rightarrow v}^{(\ell)}, \quad (1)$$

where $\mathcal{N}(x)$ denotes the neighbors of node x , $S_{c',v}$ is the (c', v) entry of \mathbf{S} , and $\bar{w}_v^{(\ell)}$, $w_{c' \rightarrow v}^{(\ell)}$ are trainable channel and CN weights, respectively. When all weights are set to 1, the NBP decoder reduces to the BP decoder. The weight set, $\mathcal{W} = \{\bar{w}_v^{(\ell)}, w_{c' \rightarrow v}^{(\ell)}\}$, is optimized via gradient descent on the unrolled neural network [30]. The loss function is designed to enhance the decoding performance [31, 32]. After training, the optimized weights are applied to the Tanner graph. Since the additional computation over BP arises only from the weighted summation in Eq. (1), the NBP decoder maintains nearly the same computational complexity of BP.

After the VN update, each CN computes its message $m_{c \rightarrow v}^{(\ell)}$ through the belief quantization step and min-sum rule [24]. At each iteration, the posterior LLR for VN v with error type ζ is computed as

$$m_{v(\zeta)} = \bar{w}_v^{(\ell)} L_{v(\zeta)} + \sum_{\substack{c' \in \mathcal{N}(v) \\ \langle \zeta, S_{c',v} \rangle = 1}} w_{c' \rightarrow v}^{(\ell)} m_{c' \rightarrow v}^{(\ell)}.$$

The estimated error operator $\hat{\mathcal{E}}$ is determined for each VN v : it is set to I if $m_{v(\zeta)} > 0$ for all ζ , and otherwise to the $\arg \min_{\zeta} m_{v(\zeta)}$. From $\hat{\mathcal{E}}$, the corresponding syndrome $\hat{\mathbf{s}}$ is computed. If $\hat{\mathbf{s}} \neq \mathbf{s}$, decoding proceeds up to $\bar{\ell}$ iterations. When no syndrome-matching operator is found after $\bar{\ell}$ iterations, a flagged failure is declared.

Algorithm 1: DE for the EBP+OSD decoder

Initialization: Randomly generate \mathcal{W}_t for $1 \leq t \leq T$

for $g = 1$ **to** G **do**

for $t = 1$ **to** T **do**

 /* Mutation */

 Generate a mutant instance $\bar{\mathcal{W}}_t$ as

$$\bar{\mathcal{W}}_t = \mathcal{W}_{t_1} + 0.5(\mathcal{W}_{t_2} - \mathcal{W}_{t_3}), \quad (2)$$

 where t_1, t_2, t_3 are randomly chosen indices.

 /* Crossover */

 Generate a trial instance $\hat{\mathcal{W}}_t$:

$$\hat{\mathcal{W}}_{t,i} = \begin{cases} \bar{\mathcal{W}}_{t,i}, & \text{with probability } p_c, \\ \mathcal{W}_{t,i}, & \text{otherwise.} \end{cases} \quad (3)$$

 /* Selection */

 Run EBP+OSD with \mathcal{W}_t and $\hat{\mathcal{W}}_t$. If $\hat{\mathcal{W}}_t$ achieves a lower LER_+ , replace \mathcal{W}_t with $\hat{\mathcal{W}}_t$.

Output: Choose \mathcal{W}_{opt} with the minimum LER_+

Conversely, when $\hat{\mathbf{s}} = \mathbf{s}$, decoding succeeds if $\mathcal{E}\hat{\mathcal{E}} \in \mathcal{S}$; otherwise, it is regarded as an unflagged failure. The overall decoding failure rate is referred to as the LER.

Upon a flagged failure in the BP or NBP decoder, a post-decoder can be activated. In this setup, the BP or NBP decoder acts as a pre-decoder, and the overall scheme is referred to as a pre+post decoder. Among various post-decoders, the OSD algorithm is widely used as a post-decoder in quantum codes. It takes the posterior LLRs $m_{v(\zeta)}$ as input and guarantees a syndrome-matching output $\hat{\mathcal{E}}$ [21]. Let UFR and FFR denote the unflagged and flagged failure rates, respectively. Then, the LER of the pre+OSD decoder, denoted by LER_+ , is expressed as

$$\text{LER}_+ = \text{UFR}_{\text{Pre}} + \text{FFR}_{\text{Pre}} \times \text{UFR}_{\text{OSD}},$$

where FFR_{Pre} represents the activation probability of the OSD stage. Although the OSD stage is crucial for achieving a lower LER_+ , it involves computationally demanding operations such as sorting, Gaussian elimination, and re-encoding.

Evolutionary BP— In the pre+OSD decoding structure, an effective pre-decoder should aim to: (i) refine the inputs to OSD to achieve a lower LER_+ and (ii) reduce the activation probability of OSD, FFR_{Pre} , thereby decreasing complexity. Unlike the BP decoder, whose structure is fixed, the NBP decoder can adapt its trainable weights to meet these objectives. However, designing a loss function that explicitly encourages such behavior remains a challenging problem. Moreover, directly training the NBP+OSD decoder to minimize LER_+ is infeasible because OSD includes inherently non-differentiable operations.

To address this limitation, we propose the EBP decoder as an end-to-end optimizable pre-decoder in conjunction with the post-OSD stage. The EBP decoder optimizes the weight set \mathcal{W} using the DE algorithm, which

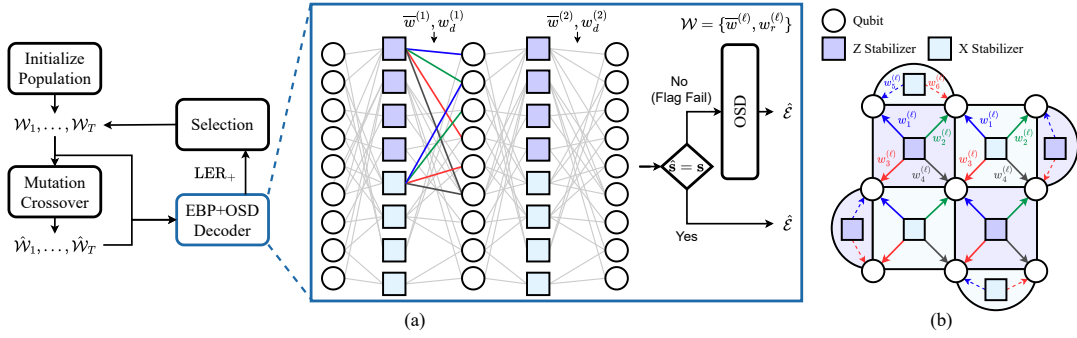


FIG. 1. (a) DE algorithm optimizing the weight set \mathcal{W} inside the EBP decoder, where the optimization explicitly targets the overall EBP+OSD performance LER_+ rather than the standalone EBP performance. (b) Surface code with $d = 3$ illustrating the weight-sharing technique, where edges of the same color share identical weights.

offers key advantages over neural networks: it can handle non-differentiable optimization problems and enables flexible objective function design. Analogous to NBP, named for its use of neural networks, EBP derives its name from the use of evolutionary algorithms for weight optimization.

The proposed DE-based optimization for the EBP decoder is summarized in Algorithm 1 and Fig. 1(a). Initially, a population of T random weight sets \mathcal{W}_t is generated. Each individual weight set then evolves for G generations through three main steps: mutation, crossover, and selection. In the mutation step, a mutant instance $\hat{\mathcal{W}}_t$ is generated from the current individual \mathcal{W}_t and two distinct individuals \mathcal{W}_{t_1} and \mathcal{W}_{t_2} according to Eq. (2). During the crossover step, a trial instance $\hat{\mathcal{W}}_t$ is formed by replacing each element of \mathcal{W}_t with the corresponding element of $\hat{\mathcal{W}}_t$ with probability p_c , as described in Eq. (3). In the selection step, both \mathcal{W}_t and $\hat{\mathcal{W}}_t$ are evaluated using the EBP+OSD decoder, where LER_+ is estimated through 100,000 Monte Carlo trials with the fixed error probability $p = p_e$. If the trial instance achieves a lower LER_+ than the current one, \mathcal{W}_t is replaced with $\hat{\mathcal{W}}_t$ for the next generation. This evolutionary update is repeated for G generations, and the instance with the best performance across all weight sets is selected as the final solution. In our implementation, the DE hyperparameters are set to $T = 500$, $G = 200$, $p_c = 0.7$, and $p_e = 0.1$.

Although the DE algorithm is a powerful tool for optimizing non-differentiable problems, it tends to converge to a local optimum when too many weights are optimized simultaneously. To substantially reduce the number of weights, we employ a weight sharing technique. For VN weights, we adopt spatial sharing [37], i.e., $\bar{w}_v^{(\ell)} = \bar{w}^{(\ell)}$ for all VNs within iteration ℓ . For CN weights $w_{c \rightarrow v}^{(\ell)}$, however, applying spatial sharing can cause message trapping across symmetric structures in quantum codes [38].

To address this issue, we introduce an edge-indexed weight-sharing scheme, where weights assigned to edges in a CN are shared by all other CNs with the same degree. Assume that the code contains two CN degree types, r_1

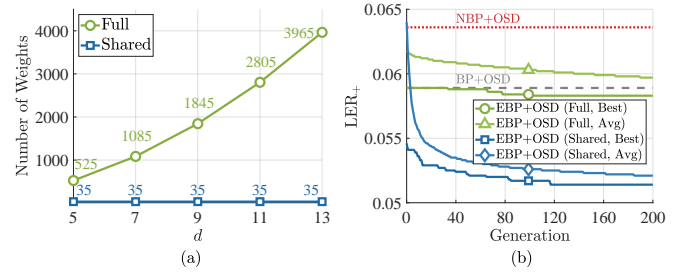


FIG. 2. Effect of the proposed sharing technique: (a) The number of weights is greatly reduced and remains constant across different d in surface codes. (b) This reduction accelerates DE convergence and yields lower LER_+ for $d = 7$.

and r_2 , as in surface and QLDPC codes. For example, the surface code with $d = 3$ in Fig. 1(b) includes four CNs with $r_1 = 4$ and four CNs with $r_2 = 2$. The edge-indexed sharing scheme defines a weight set $\{w_1^{(\ell)}, \dots, w_{\bar{r}}^{(\ell)}\}$ for $\bar{r} = r_1 + r_2$. The first r_1 weights correspond to CNs with degree r_1 , and the next r_2 weights correspond to CNs with degree r_2 . Each edge uses a weight determined by its local index; for instance, the second edge of a degree- r_1 CN uses $w_2^{(\ell)}$, whereas the second edge of a degree- r_2 CN uses $w_{r_1+2}^{(\ell)}$. Accordingly, the proposed sharing method reduces the weight set to

$$\mathcal{W} = \{\bar{w}^{(\ell)}, w_r^{(\ell)} | 1 \leq \ell \leq \bar{\ell}, 1 \leq r \leq \bar{r}\}.$$

In Fig. 1(b), for degree-4 CNs, solid edges of the same color share the identical weight, while dashed edges connected to degree-2 CNs also share weights by colors, following the same principle.

Fig. 2(a) compares the numbers of weights in surface codes for $\bar{\ell} = 5$, without and with weight sharing (denoted as Full and Shared, respectively) as a function of d . Without sharing, the number of weights increases quadratically with d , whereas the weight sharing method keeps it constant as $\bar{\ell} \times (\bar{r} + 1)$ for all d . This implies that a single weight set can be reused across surface codes. Fig. 2(b) shows the evolution of LER_+ for the

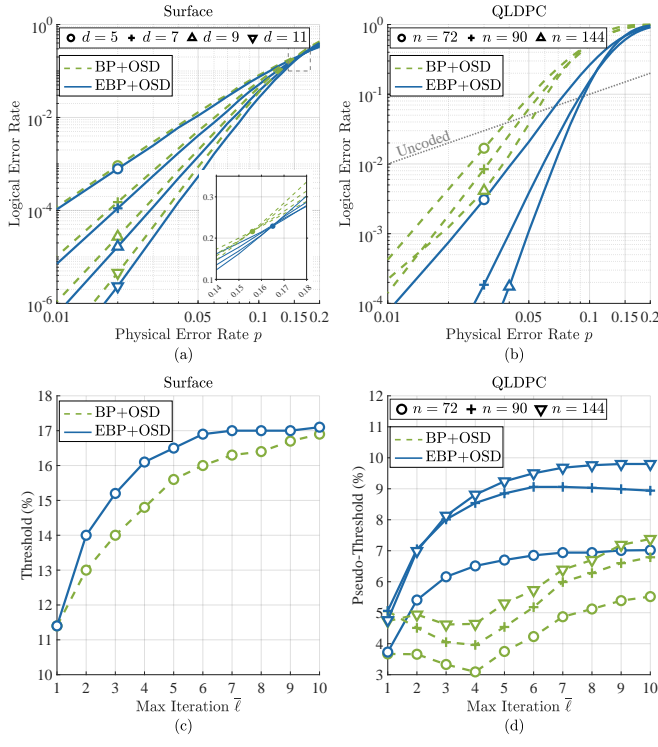


FIG. 3. Performance comparison between BP+OSD and EBP+OSD for surface codes (left column) and QLDP codes (right column) in terms of LER (upper row) and threshold (lower row).

surface code with $d = 7$ at $p = 0.1$, demonstrating that weight sharing accelerates the convergence of the DE algorithm. Without sharing, the average LER_+ across all instances (Avg) fails to converge to the best result (Best), while with sharing, the Avg and Best curves align closely. In addition, the EBP+OSD decoder with the optimized weight set significantly outperforms baseline decoders such as BP+OSD and NBP+OSD decoders.

Furthermore, we introduce an additional selection criterion in the DE algorithm to reduce complexity: if the difference in values of LER_+ from \mathcal{W}_t and $\hat{\mathcal{W}}_t$ is within 1%, but $\hat{\mathcal{W}}_t$ achieves a lower FFR_{Pre} , $\hat{\mathcal{W}}_t$ is selected. In addition, to enhance convergence of the DE algorithm, we adopt the best/1/bin strategy [34] after half of the generations, which enables DE to converge to a single optimized solution.

Results— Fig. 3 compares performances of the BP+OSD and the proposed EBP+OSD decoders for the surface codes (left column) and QLDP codes (right column) in terms of the LER (upper row) and threshold (lower row). The results in Figs. 3(a) and (b) are obtained under a depolarizing noise model with $\bar{\ell} = 5$. Using the edge-indexed sharing method, we optimize the weight set using the surface code with $d = 7$ and reuse it for other surface codes. Similarly, for QLDP codes, we optimize the weights only for the code with $n = 72$ and reuse them for the QLDP codes with $n = 90$ and

TABLE I. Threshold comparison of various decoders

Decoder	Iteration $\bar{\ell}$	Threshold	Pseudo-Threshold	
		Surface	Surface	QLDPC
MWPM [39]	—	14.7%	11.9%	—
FFNN [26]	—	—	12.4%	—
CNN [27]	—	—	11.9%	—
CNN [28]	—	—	13.2%	—
AMBp [36]	150	16.0%	—	—
BP+TBD [35]	20	15.8%	—	—
BP+OSD [21]	5	15.6%	12.9%	3.8%
EBP+OSD	5	16.5%	13.7%	6.7%
EBP+OSD	10	17.1%	13.8%	7.0%
EBP+OSD	10	17.1%	13.8%	9.8%

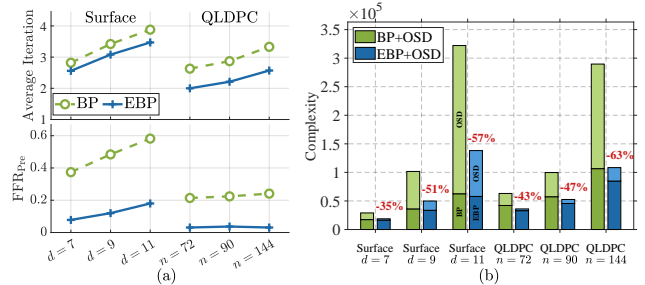


FIG. 4. Comparison of decoding complexity between BP+OSD and EBP+OSD decoders: (a) EBP consistently reduces the average iteration count and FFR_{Pre} for surface and QLDP codes. (b) EBP+OSD achieves a 35–63% reduction in total complexity across all codes.

$n = 144$, which significantly reduces optimization time. In Fig. 3(a), the EBP+OSD decoder achieves consistent LER improvement across all code distances d for the surface codes, increasing the threshold from 15.6% to 16.5%. Fig. 3(c) presents the threshold as a function of $\bar{\ell}$, where a substantial improvement is observed for low iteration counts, demonstrating that EBP+OSD is particularly effective for low-latency decoding scenarios.

For QLDP codes, as shown in Fig. 3(b), the LER improvement achieved by the EBP+OSD decoder is even more pronounced. In Fig. 3(d), the pseudo-threshold (the intersection with the physical error rate) improves by several percentage points at low $\bar{\ell}$. Interestingly, the BP+OSD decoder does not exhibit a monotonic threshold increase with additional iterations $\bar{\ell}$, suggesting that a stronger pre-decoder with higher $\bar{\ell}$ alone does not necessarily yield optimal performance in a pre+OSD decoder. In contrast, the EBP+OSD decoder demonstrates an almost monotonic threshold improvement, as its weights are optimized to maximize the overall pre+OSD decoder performance. Table I further compares the threshold performance with those of existing decoders. For both surface and QLDP codes, the EBP+OSD decoder achieves state-of-the-art performance, even with only 5 iterations.

In Fig. 4, we evaluate the total computational complexity of the BP+OSD and EBP+OSD decoders at

$p = 0.05$ and $\bar{\ell} = 5$, measured in equivalent addition operations [40]. To enable a fair comparison of average complexity, the pre-decoder complexity is computed as the product of the average number of iterations and the per-iteration complexity, while the OSD complexity is weighted by the OSD activation probability FFR_{Pre} . As shown in Fig. 4(a), both the average number of iterations and FFR_{Pre} are reduced for the EBP decoder compared with the BP decoder. Consequently, Fig. 4(b) shows that, across all codes, the EBP+OSD decoder achieves a total complexity reduction ranging from at least 35% to as much as 63%.

Conclusion— Although the BP+OSD decoder demonstrates strong performance across various quantum codes, it has not been explicitly optimized and remains

computationally expensive. To address this limitation, we introduce the EBP decoder—an end-to-end optimizable pre-decoder trained using the DE algorithm. The flexibility of DE enables effective optimization that jointly considers decoding performance and computational complexity, even with the non-differentiable OSD stage. As a result, the EBP+OSD decoder achieves significant improvement in both decoding performance and complexity reduction under low-latency conditions. For surface codes, it yields a 0.9% threshold gain and up to a 57% reduction in complexity, while for QLDPC codes, it provides a 2.9–3.9% threshold gain with up to a 62% reduction in complexity. To the best of our knowledge, this is the first work to enhance BP decoding through evolutionary optimization, underscoring its potential to advance practical, low-latency quantum decoders.

[1] P. W. Shor, Polynomial-time algorithms for prime factorization and discrete logarithms on a quantum computer, *SIAM Rev.* **41**, 303 (1999).

[2] A. Aspuru-Guzik, A. D. Dutoi, P. J. Love, and M. Head-Gordon, Simulated quantum computation of molecular energies, *Science* **309**, 1704 (2005).

[3] C. Gidney and M. Ekerå, How to factor 2048 bit RSA integers in 8 hours using 20 million noisy qubits, *Quantum* **5**, 433 (2021).

[4] F. A. et al., Quantum supremacy using a programmable superconducting processor, *Nature* **574**, 505 (2019).

[5] P. W. Shor, Scheme for reducing decoherence in quantum computer memory, *Phys. Rev. A* **52**, R2493(R)–R2496(R) (1995).

[6] A. M. Steane, Error correcting codes in quantum theory, *Phys. Rev. Lett.* **77**, 793 (1996).

[7] A. R. Calderbank and P. W. Shor, Good quantum error-correcting codes exist, *Phys. Rev. A* **54**, 1098 (1996).

[8] D. Bluvstein and Others, Logical quantum processor based on reconfigurable atom arrays, *Nature* **626**, 58 (2024).

[9] S. Bravyi, A. W. Cross, J. M. Gambetta, D. Maslov, P. Rall, and T. J. Yoder, High-threshold and low-overhead fault-tolerant quantum memory, *Nature* **627**, 778 (2024).

[10] R. A. et al., Suppressing quantum errors by scaling a surface code logical qubit, *Nature* **614**, 676 (2023).

[11] Google Quantum AI, Suppressing quantum errors by scaling a surface code logical qubit, *Nature* **614**, 676 (2023).

[12] Google Quantum AI, Quantum error correction below the surface code threshold, *Nature* **638**, 920 (2024).

[13] B. M. Terhal, Quantum error correction for quantum memories, *Rev. Mod. Phys.* **87**, 307 (2015).

[14] R. G. Gallager, Low-density parity-check codes, *IRE Trans. Inf. Theory* **8**, 21 (1962).

[15] A. Y. Kitaev, Fault-tolerant quantum computation by anyons, *Annals of Physics* **303**, 2 (2003).

[16] E. Dennis, A. Kitaev, A. Landahl, and J. Preskill, Topological quantum memory, *J. Math. Phys.* **43**, 4452 (2002).

[17] S. B. Bravyi and A. Y. Kitaev, Quantum codes on a lattice with boundary, arXiv preprint (1998), arXiv:quant-ph/9811052 [quant-ph].

[18] A. G. Fowler, M. Mariantoni, J. M. Martinis, and A. N. Cleland, Surface codes: Towards practical large-scale quantum computation, *Phys. Rev. A* **86**, 032324 (2012).

[19] D. J. C. MacKay, G. Mitchison, and P. L. McFadden, Sparse-graph codes for quantum error correction, *IEEE Trans. Inf. Theory* **50**, 2315 (2004).

[20] P. Panteleev and G. Kalachev, Quantum ldpc codes with almost linear minimum distance, *IEEE Trans. Inf. Theory* **68**, 213 (2021).

[21] P. Panteleev and G. Kalachev, Degenerate quantum ldpc codes with good finite length performance, *Quantum* **5**, 585 (2021).

[22] D. Poulin and Y. Chung, On the iterative decoding of sparse quantum codes, *Quantum Inf. Comput.* **8**, 987 (2008).

[23] Z. Babar, P. Botsinis, D. Alanis, S. X. Ng, and L. Hanzo, Fifteen years of quantum ldpc coding and improved decoding strategies, *IEEE Access* **3**, 2492 (2015).

[24] C.-Y. Lai and K.-Y. Kuo, Log-domain decoding of quantum ldpc codes over binary finite fields, *IEEE Transactions on Quantum Engineering* **2**, 1 (2021).

[25] J. Roffe, D. R. White, S. Burton, and E. T. Campbell, Decoding across the quantum ldpc code landscape, *Phys. Rev. Research* **2**, 043423 (2020).

[26] S. Varsamopoulos, B. Criger, and K. Bertels, Decoding small surface codes with feedforward neural networks, *Quantum Sci. Technol.* **3**, 015004 (2017).

[27] C. Chamberland and P. Ronagh, Deep neural decoders for near term fault-tolerant experiments, *Quantum Sci. Technol.* **3**, 044002 (2018).

[28] H. Jung, I. Ali, and J. Ha, Convolutional neural decoder for surface codes, *IEEE Transactions on Quantum Engineering* **5**, 3102513 (2024).

[29] J. B. et al., Learning high-accuracy error decoding for quantum processors, *Nature* **635**, 834 (2024).

[30] E. Nachmani, E. Marciano, L. Ligosch, W. J. Gross, D. Burshtein, and Y. Be'ery, Deep learning methods for improved decoding of linear codes, *IEEE J. Sel. Top. Signal Process.* **12**, 119 (2018).

[31] Y.-H. Liu and D. Poulin, Neural belief-propagation decoders for quantum error-correcting codes, *Phys. Rev.*

Lett. **122**, 200501 (2019).

[32] S. Miao, A. Schnerring, H. Li, and L. Schmalen, Quaternary neural belief propagation decoding of quantum ldpc codes with overcomplete check matrices, IEEE Access **11**, 1 (2025).

[33] R. Storn and K. Price, Differential evolution—a simple and efficient heuristic for global optimization over continuous spaces, J. Global Optim. **11**, 341 (1997).

[34] S. Das and P. N. Suganthan, Differential evolution: A survey of the state-of-the-art, IEEE Trans. Evol. Comput. **15**, 4 (2011).

[35] H. Jung and J. Ha, Topological blocking decoder for surface codes, Phys. Rev. A **111**, 042424 (2025).

[36] K.-Y. Kuo and C.-Y. Lai, Exploiting degeneracy in belief propagation decoding of quantum codes, npj Quantum Information **8**, 111 (2022).

[37] J. Dai, K. Tan, Z. Si, K. Niu, M. Chen, H. V. Poor, and S. Cui, Learning to decode protograph LDPC codes, IEEE J. Sel. Areas Commun. **39**, 1956 (2021).

[38] N. Raveendran and B. Vasić, Trapping sets of quantum LDPC codes, Quantum **5**, 562 (2021).

[39] J. Edmonds, Paths, trees, and flowers, Can. J. Math. **17**, 449 (1965).

[40] H. Gamage, N. Rajatheva, and M. Latva-Aho, Channel coding for enhanced mobile broadband communication in 5G systems, in *Proc. Eur. Conf. Netw. Commun. (EuCNC)* (2017) pp. 1–6.